MIT Libraries | DSpace@MIT

MIT Open Access Articles

Plasma-Density Determination from X-Ray Radiography of Laser-Driven Spherical Implosions

Massachusetts Institute of Technology

Plasma-Density Determination from X-Ray Radiography of Laser-Driven Spherical Implosions

F. J. Marshall, P. W. McKenty, J. A. Delettrez, R. Epstein, J. P. Knauer, and V. A. Smalyuk

Laboratory for Laser Energetics, University of Rochester 250 E. River Road, Rochester, New York 14623, USA

J. A. Frenje, C. K. Li, R. D. Petrasso, and F. H. Séguin

Plasma Science and Fusion Center, Massachusetts Institute of Technology, Cambridge, Massachusetts 02139, USA

R. C. Mancini

Department of Physics, University of Nevada, Reno, Nevada 89557, USA

The fuel layer density of an imploding laser-driven spherical shell is inferred from framed x-ray radiographs. The density distribution is determined by using Abel inversion to compute the radial distribution of the opacity κ from the observed optical depth τ. With the additional assumption of the mass of the remaining fuel, the absolute density distribution is determined. This is demonstrated on the OMEGA laser system with two x-ray backlighters of different mean energies that lead to the same inferred density distribution independent of backlighter energy.

Inertial confinement fusion (ICF) relies on the compression of spherical targets by means of a high power driver, such as a laser, to achieve the necessary conditions of high density and temperature [1]. Areal densities of ~ 0.3 g/cm^2 and temperatures of ~ 10 keV must be obtained in the central hot spot for ignition to occur. Measurements of the target areal density provide a means of comparing the actual and predicted conditions in ICF implosions.

Previous experiments performed with the OMEGA laser [2] have been successful in inferring the areal density of the imploding capsule at the time of fusion particle production [3–5] (hot-spot formation). At this time, the hot-spot temperature is at maximum, whereas the cold main fuel layer is still evolving. The total areal density of the capsule is determined from the slowing down of protons resulting from D-^{3}He fusion reactions within the fuel. These can be either primary fusion reactions from a D^{3}He gas fill or secondary reactions from a D$_2$ gas fill. This method determines the total areal density by associating proton energy loss with the amount of plasma traversed. This method is restricted to sampling the areal density at the time of fusion particle production.

In non-igniting capsules, the cold main fuel layer produces negligible fusion yield and emitted radiation. It is therefore difficult to diagnose. The problem is solved by the introduction of an outside source of radiation (backlighter) acting as a probe. Both x-ray [6] and proton backlighters [7] have been employed as plasma probes in laser-driven fusion experiments. X-ray backlighters have been extensively used for both planar experiments and spherical implosions on OMEGA. X-ray backlighting of spherical implosions on OMEGA has been restricted to experiments using fewer than 60 beams to drive the target implosion,

freeing up some of the beams to generate the x-ray backlighter emission. The recent completion of the OMEGA EP laser [8] will make it possible to generate a backlighter while using all 60 OMEGA beams to drive the implosion.

In this work, it is shown that the density distribution of the plasma can be inferred from framed x-ray radiographs. With x-ray backlighter emission available during and after core formation, the time history of the main fuel layer density, and therefore the areal density, can be determined. The use of two-dimensional imaging techniques such as pinhole imaging, Kirkpatrick-Baez microscopes, and Bragg crystal diffraction are preferred since there may be significant azimuthal variation of the plasma density.

In a previous treatment of this problem [9], a Ge-doped ablator at a temperature $\ll 100$ eV was assumed to have the opacity of cold matter. The imploding shell, driven by a hohlraum, was radiographed with a nearly monochromatic Ti x-ray backlighter at conditions close to that of the Ti backlighter used in this work. The density of the pusher was inferred from the radiographs using this assumption of cold opacity and Abel inversion. It is shown here that by constraining the mass to that of the unablated shell mass, the absolute density determined is independent of the backlighter spectrum, relaxing the need to precisely know the opacity of the plasma. This is demonstrated using x-ray radiographs of polar-driven implosions [10] performed on OMEGA with an Au backlighter (broadband emission from ~ 2.5 to 4.5 keV) and a Ti backlighter (with emission from ~ 4.7 to 5 keV). Despite a significant difference of the magnitude of the plasma opacity resulting from these two backlighters, the method yields the same density distribution when simultaneous framed images are compared.

For a radially symmetric distribution, absorption of backlighter x rays along the line of sight, in the direction

z, is given by

$$I = I_0 \exp\left[-\int \kappa(E, r)dz\right], \quad (1)$$

where I is the observed intensity, I_0 is the backlighter intensity, and κ is the opacity in cm^{-1} at energy E and radius r ($r^2 = y^2 + z^2$, y is the projected radial position). The opacity can also be expressed as $\kappa(E, r) = \mu(E, r) \rho(r)$ where μ is the mass absorption coefficient in cm^2/g and ρ is the density in g/cm^3. The integral in Eq. (1) is the Abel transform [11] of the opacity. When the inverse Abel transform [11] is applied to Eq. (1), the result is an expression for the radially dependent opacity as a function of the observed intensity at y

$$\kappa(E, r) = \frac{1}{\pi} \int_r^\infty \frac{d}{dy}\left\{\ln\left[\frac{I(y)}{I_0}\right]\right\} \frac{dy}{\sqrt{y^2 - r^2}}. \quad (2)$$

The mass absorption coefficient $\mu(E)$ at energy E can be assumed to be approximately constant through the absorbing region of the plasma if the temperature and density are sufficiently low. This has been shown to be the case in a CH plasma [12] for temperatures below ~ 100 eV and densities below ~ 100 g/cm^3 where bound-free absorption [13] by carbon K-shell electrons dominates. In such a case, the mass absorption coefficient averaged over the energy band of the radiograph $\mu_{eff}(E)$ can be used to infer the absolute density from $\rho(r) = \kappa(E, r)/\mu_{eff}(E)$. Uncertainties in the instrumental response or an incomplete knowledge of the spectral shape can make it difficult to determine the exact value of $\mu_{eff}(E)$. If, however, the mass of the plasma shell M_{shell} is known, then $\mu_{eff}(E)$ can be determined from

$$M_{shell} = \int \rho(r)dV = 4\pi \int \frac{\kappa(E, r)}{\mu_{eff}(E)} r^2 dr. \quad (3)$$

By choosing M_{shell} to be the unablated mass obtained from simulation, the absolute density is then determined. Fujioka *et al.* [14] have shown that absorption of x rays from a Ti backlighter (one of two used in this work) by polystyrene (CH) can indeed be characterized by an effective energy-band-dependent absorption coefficient.

If the absorber is fully stripped, as is the case for a pure-hydrogen fuel layer, and is at a sufficiently high temperature, as would be expected for a D or DT main fuel layer near stagnation, the opacity is $\propto \rho^2/T^{1/2}$ and, therefore, the optical depth is $\propto \rho^2 R/T^{1/2}$ [15,16], where T is the temperature and R is the radius. If the temperature variation of the absorber is small, the radial variation of the opacity can be determined by Abel inversion from which a functional form of the density distribution can be determined. Constraining the mass to that of the unablated shell mass allows the absolute density distribution as a function of radius to be calculated.

Experiments were performed using 40 beams of the OMEGA laser in the polar-drive illumination configuration [10], emulating the conditions on the NIF (the National Ignition Facility) [17] when direct-drive implosions are performed with the beams in the indirect-drive configuration. The beam pointing used was described in Marshall *et al.* [10] (case 3, with offsets of rings 1, 2, and 3 of 90, 150, and 150 μm, respectively) on a target with an outer radius of 433 μm. The target consisted of a 24-μm-thick glow-discharge-polymer GDP (i.e., CH) shell filled with 15 atm of D_2 at room temperature. The main drive pulse consisted of a 1.5 ns pulse with a 1-to-3 (foot-to-main) intensity ratio with the foot and main part of the pulse having approximately equal durations (~ 0.75 ns). A total of 13.2 kJ was incident on the target with 1-THz bandwidth smoothing by spectral dispersion (SSD) [18] with polarization smoothing [19] used to minimize small-scale illumination nonuniformities. This pulse shape was used to keep the main fuel layer on a low adiabat ($P/P_{Fermi} \sim 3$) [1].

Two backlighter targets were employed opposite two high-speed x-ray framing cameras [20]. One backlighter was a 25-μm-thick Au foil and the other a 25-μm-thick Ti foil, each with four OMEGA beams of ~ 350 J/beam, focused to diameters of 750 and 600 μm, respectively. Each framing camera was positioned behind a 4×4 array of 10-μm-diam pinholes producing four strips of framed images with a time-gated resolution of ~ 30 ps, 56 ps between images, and strip times independently set to the nearest 100 ps. Absolute frame times were determined by observing the backlighter onset on the first strip and from the measured delay from strip to strip determined from an electronically recorded monitor signal.

The framing camera opposite the Au backlighter was filtered with a total of 229 μm of Be making it possible for x rays above ~ 2.5 keV to be transmitted. The framing camera opposite the Ti backlighter was filtered with a 12.7-μm-thick Ti filter. This filter limits the transmitted spectrum of the backlighter so as to be nearly monoenergetic with a characteristic energy of 4.75 keV, corresponding to the He-like emission line of Ti [9]. This simplifying assumption about the backlighter spectrum will be used later in this Letter as a means of checking the accuracy of the assumed mass of the shell.

The images are recorded on film with an imposed step wedge so that relative intensity variations can be determined. The exposed images and step wedge are developed simultaneously to make possible the subsequent conversion to intensity variation from scanned and digitized film. Variations of the backlighter intensity are removed by fitting the shape of the backlighter to a super-Gaussian-plus background outside the region of the target radiograph and then extending this fit to the region of the radiograph [21].

Figure 1 shows a set of these corrected radiographs up to shell stagnation, which occurs at ~ 2.3 ns. Note that all images are during the time period after the end of the laser pulse ($t \sim 1.5$ ns) at which time all ablation has already occurred and it is assumed that the mass of the shell then remains constant. The values are presented as $-\ln(I/I_0)$ [i.e., the optical depth τ]; all values are >0 with the
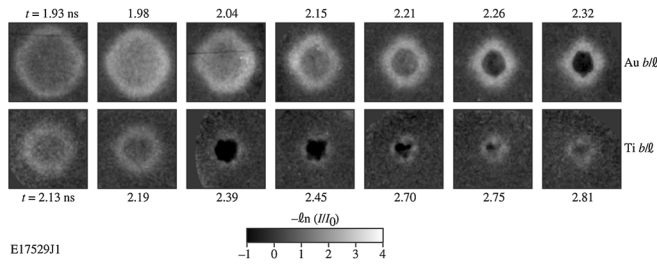
FIG. 1. Intensity-corrected x-ray radiographs from OMEGA shot 49331 taken with two x-ray framing cameras, one backlit by an Au target and one backlit by a Ti target. Each image is a 400×400-μm region corrected for backlighter intensity variation as explained in the text.

exception of the frames from 2.32 ns and on where self-emission from the core exceeds emission from the backlighter in the central region of the images. Figure 2(a) shows the azimuthally averaged optical-depth variation for one nearly simultaneous pair (at the mean time of $t = 2.14$ ns) of Au- and Ti-backlit images. The magnitude of the optical depth is greater for the lower-energy backlighter as expected. The dotted line in Fig. 2(a) is the Au-backlit profile divided by 1.7 showing that the optical depths differ only by a multiplicative constant. Applying Abel inversion
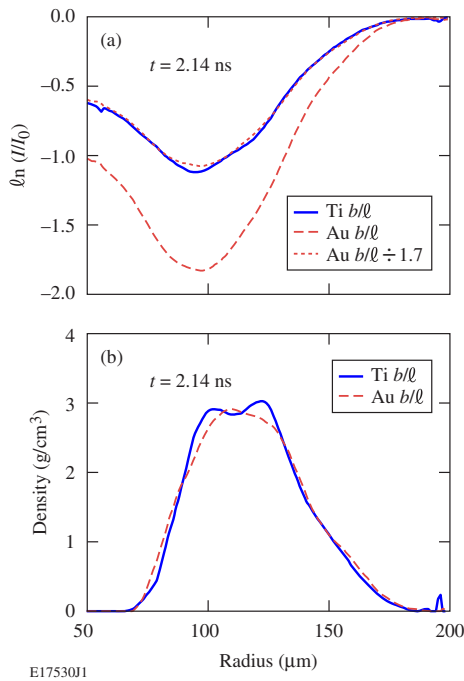

FIG. 2 (color online). (a) The natural logarithm of the intensity variation as a function of projected radial distance in the image plane for a simultaneous pair of Au- and Ti-backlit images. The profiles are azimuthally averaged about the image centers. The dotted line is the Au profile, normalized to the Ti profile demonstrating that they differ only by a multiplicative constant (1.7). (b) The absolute density distributions computed from the intensity profiles of (a) by Abel inversion with the additional constraint of mass as described in the text.

and assuming the unablated shell mass (3.34×10^{-5} g) given by the 1D hydrodynamic code LILAC [22] determines the density distributions from the observed optical depths [Fig. 2(b)]. The inferred density distributions from the Au and Ti backlighters are nearly identical, with only small differences due to noise in the images.

An independent check on the accuracy of the assumed mass can be obtained by determining the areal density of the shell from the transmission through the center of the shell. For the nearly monoenergetic Ti backlit image [Fig. 2(b)], the observed optical depth near the center of the image is 0.63. For a cold opacity of 19.72 cm^2/g [14], the areal density is then $\rho R = \tau/2\mu = 16$ mg/cm^2, within $\sim$14% of the value obtained from the Abel inverted profile ($\rho R = 18.5$ mg/cm^2). In general, the Abel inversion result will average over more of the shell and hence will be less subject to local variations of the areal density.

Figure 3 shows the density distributions determined for a sample of these images. The densities inferred from one additional simultaneous pair of Au- and Ti-backlit images are included. The LILAC simulated shell density is shown for comparison for the 2.20-ns case. Figure 4 shows the resulting calculated shell areal densities ρR_{shell} determined from all Au- and Ti-backlit images plotted as a function of frame time from the beginning of the main laser pulse ($t = 0$). For the two frames when the Au- and Ti- backlit images occurred at the same time, the areal density values are the same within errors. All times have an uncertainty of ± 50 ps. The absolute densities and, therefore, the areal densities are assumed to be uncertain by ± 10% due to uncertainty in the unablated mass. The time from $\sim$2.3 to 2.6 ns corresponds to the time during which intense x-ray emission from the core as well as fusion production occurs. During peak emission, heat from the core moves out through the shell and absorption by the backlighter is momentarily obscured. Since an independent measurement of this emission is not available (image with no backlighter), it cannot be corrected for and no density profiles are determined during this time interval. Later in time, the shell cools and absorption of the backlighter reappears.
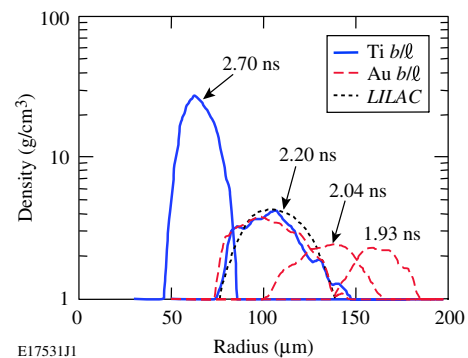

FIG. 3 (color online). Density distributions computed from the x-ray radiographs showing the evolution of the shell density and position as a function of the indicated frame times.
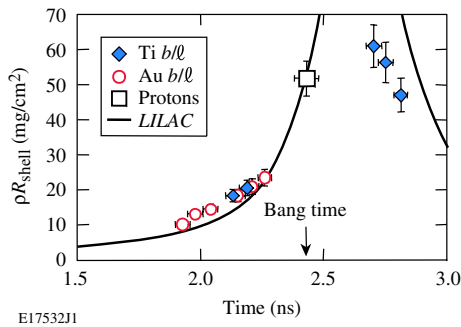
E17532J1

FIG. 4 (color online).   The shell areal densities computed from all available x-ray radiographs including those where the emission from the core is just starting (2.3 ns) and as core emission subsides (2.6 ns and later). The value determined from the proton spectra is plotted at the time of peak neutron emission (2.43 ns). The LILAC-simulated shell areal density, shown as a solid line, reached a peak of 110 mg/cm^2 at 2.64 ns (off scale).

Frames during this later time were recorded by the Ti-backlit framing camera (2.70 ns and later).

The mean neutron production time (bang time), as recorded by the neutron temporal diagnostic [23], occurred at 2.43 ns during the time interval when x-ray emission from the core is evident. The total areal density (gas-fill + shell) averaged over the time of fusion particle production was independently determined by a set of three filtered CR39 packs measuring the slowing down of the D-He^3 protons [3] and yields a value of $\langle\rho R\rangle_p = 58 \pm 5$ mg/cm^2 (the error is 1 standard deviation of the three values). An estimate of the gas-fill (fuel) areal density ρR_{fuel} is determined from the size of the observed core emission at stagnation ($\sim$50 μm) and mass conservation, yielding $\rho R_{fuel} = 6 \pm 1$ mg/cm^2. The proton inferred shell areal density is therefore $\langle\rho R_{shell}\rangle_p = 52 \pm 5$ mg/cm^2 and is plotted as a single point in Fig. 4 at bang time. The value determined from the proton spectra falls closely on the trend of the x-ray measurements, giving additional credence to the results of this method. The LILAC simulation of this implosion was performed assuming flux-limited diffusion [24] with a flux limiter $f = 0.06$. The predicted areal density is shown as a solid line in Fig. 4. The areal density measurements are seen to closely follow this prediction until the time of stagnation where significant departures from spherical symmetry can be seen in the framed images (Fig. 1).

This analysis demonstrates that with the application of an area x-ray backlighter, the shell areal density time history can be measured on a single implosion experiment from early in the implosion, up to stagnation, and again later in time after core emission has subsided. Such a determination is limited by the temporal extent of the backlighter and the requisite exclusion of target self emission. A similar measurement of the areal density time history using proton radiography [7] requires repeating the implosion, acquiring a single time measurement from each of a series of identical implosions. The x-ray radiography technique therefore offers a much less intensive use of the experimental facility, not requiring that the implosion be repeated multiple times to acquire the areal density time history. The results of this technique support the conclusion that the polar-driven direct-drive implosion exhibits near 1D performance, up to the time of core self emission, with evolving nonuniformities affecting the performance thereafter. The reader is referred to the discussion in Ref. [10] for a description of the low Legendre mode departures from spherical symmetry observed in polar-driven, direct-drive implosions that are of importance to the target performance but outside the scope of this Letter.

[1] J. D. Lindl *et al.*, Phys. Plasmas **11**, 339 (2004).
[2] T. R. Boehly *et al.*, Opt. Commun. **133**, 495 (1997).
[3] F. H. Séguin *et al.*, Rev. Sci. Instrum. **74**, 975 (2003).
[4] V. A. Smalyuk *et al.*, Phys. Rev. Lett. **90**, 135002 (2003).
[5] J. A. Frenje *et al.*, Phys. Plasmas **11**, 2798 (2004).
[6] O. L. Landen *et al.*, Rev. Sci. Instrum. **72**, 627 (2001).
[7] C. K. Li *et al.*, Plasma Phys. Controlled Fusion **51**, 014003 (2009).
[8] C. Stoeckl *et al.*, Fusion Sci. Technol. **49**, 367 (2006).
[9] D. H. Kalantar *et al.*, Rev. Sci. Instrum. **68**, 814 (1997).
[10] F. J. Marshall *et al.*, J. Phys. IV (France) **133**, 153 (2006).
[11] R. N. Bracewell, *The Fourier Transform and Its Applications* (McGraw-Hill, Boston, MA, 2000), 3rd ed., pp. 351–356.
[12] F. J. Marshall *et al.*, Phys. Rev. E **49**, 4381 (1994).
[13] H. A. Bethe and E. E. Salpeter, *Quantum Mechanics of One- and Two-Electron Atoms* (Academic Press, New York, 1957), pp. 295–305.
[14] S. Fujioka *et al.*, Phys. Plasmas **10**, 4784 (2003).
[15] Ya. B. Zel'dovich and Yu. P. Raizer, *Physics of Shock Waves and High-Temperature Hydrodynamic Phenomena* edited by W. D. Hayes and R. F. Probstein (Academic Press, New York, 1966), Vol. 1, pp. 269–272.
[16] B. Yaakobi, R. Epstein, and F. J. Marshall, Phys. Rev. A **44**, 8429 (1991).
[17] W. J. Hogan *et al.*, Nucl. Fusion **41**, 567 (2001).
[18] S. Skupsky *et al.*, J. Appl. Phys. **66**, 3456 (1989).
[19] T. R. Boehly *et al.*, J. Appl. Phys. **85**, 3444 (1999).
[20] D. K. Bradley *et al.*, Rev. Sci. Instrum. **66**, 716 (1995).
[21] J. P. Knauer *et al.*, Phys. Plasmas **7**, 338 (2000).
[22] J. Delettrez *et al.*, Phys. Rev. A **36**, 3926 (1987).
[23] R. A. Lerche, D. W. Phillion, and G. L. Tietbohl, Rev. Sci. Instrum. **66**, 933 (1995).
[24] R. C. Malone, R. L. McCrory, and R. L. Morse, Phys. Rev. Lett. **34**, 721 (1975).